Characterization methods for studying protein adsorption on nano-polystyrene beads

Catia Contado [a], *, Dora Mehn [b], Douglas Gilliland [b], Luigi Calzolai [b], *

[a] *Department of Chemical and Pharmaceutical Sciences, University of Ferrara, Via Luigi Borsari 46, 44121 Ferrara, Italy*
[b] *European Commission — Joint Research Centre, Institute for Health and Consumer Protection, Nanobiolab, Via E. Fermi 2749, 21027 Ispra, VA, Italy*

ARTICLE INFO

ABSTRACT

This work is dealing with the use of polystyrene (PS) nanoparticles as substrates for bioanalytical specific interactions. Different techniques were used for the accurate characterization of the PS nanoparticles of 100 nm and 196 nm before coating them with a layer of antibodies against immunoglobulins of type E (aIgE), giving to the particle a specific functionality. The formation of the aIgE adsorbed layer was monitored using centrifugal particle separation (CPS) and centrifugal field flow fractionation (CF3) experiments, which allowed to determine the size changes and the adsorbed mass. Particle sizes were also measured with DLS, used both as stand-alone instrument and coupled to CF3 (CF3-DLS). The complementary information obtained from the CPS and CF3-DLS measurements allowed the estimation of the density of the aIgE shell. The proteins immobilized at the surface fully retained their activity, as proven by the reactions between the functionalized PS-aIgE particles and immunoglobulins of type E (IgE) dispersed in suspensions prepared on purpose.

© 2019.

1. Introduction

Protein adsorption on any foreign surface exposed to a protein solution is a spontaneous, highly favorable and often irreversible process, subject of long-standing debate, principally because of the wide range of adsorption mechanisms adopted by diverse protein structures and for the wide variety of possible surfaces either in terms of shape and chemical composition. The adsorption process is a mix of physical (electrostatic, hydrophobic, dispersion, etc.) and chemical interactions (hydrogen bonds, π–π stacking), that might lead to the formation also of real covalent bonds between the protein molecules and the surface [1].

The development and use of miniaturized medical devices, the creation of new biosensors, drug delivery nanosystems and the recent impelling interest about the presence of nano and micromaterial in the environment [2], make the study of these bio-non/bio interfaces one of the key topics in the development of nanotechnology applications.

In this work, we focus on the adsorption of immunoglobulin proteins onto synthetic polymer nanoparticles because of their potential for biomedical applications [3]. Polymeric nanoparticles offer a versatile platform for developing imaging and drug delivery applications due to the possibilities of being modified with functional moieties ranging from small chemical groups to large macromolecules. Immunoglobulins (Igs), also known as antibodies (Abs), have an extraordinary specificity and binding affinity toward antigens (Ags), thus rendering this special protein class of crucial interest for designing immunoassays, producing biosensors, chromatographic immuno-affinity columns and for biomaterials development [4]. Of the five major antibody classes identified in placental mammals (IgG, IgM, IgA, IgD and IgE) [5], IgG is the most abundant antibody in human serum (˜ 10 mg mL^{-1}, accounting for 70–85% of the total immunoglobulin pool), while IgE is very scarce (˜75 ng mL^{-1}) [6]. IgE are only found in mammals and mediate allergic response that can lead to powerful immune reactions, especially in the case of allergy classified as of "type 1" (hypersensitivity) [7,8].

To study antibody adsorption on polymeric nanoparticles is intrinsically difficult, as only a limited number of techniques are available to characterize nanoparticle-protein complexes directly in solution. The IgG adsorption mechanism on polystyrene (PS) microparticles [9] and onto negatively charged PS nanoparticles was investigated by using the electrophoretic mobility and concentration depletion methods, proving that IgG adsorption is irreversible [10–12] and that the electrophoretic mobility of PS particles increases with the increasing amount of IgG adsorbed onto the surface until it reaches a plateau values [13]. The amount of Igs adsorbed onto latex particles was determined in the past with the centrifugal field flow fractionation (CF3) technique [14–17] and more recently, with a suspended microchannel resonator (SMR) [18]. The mass variation of a particle due to the protein adsorption can be monitored also with the centrifugal particle sedimentation (CPS, reported in the literature as differential centrifugal sedimentation DCS or disk centrifuge, Photosedimentometry DCP, descending from the Joyce-Loebl disc centrifuge) [19–21], however CPS was used to determine the amount of Igs adsorbed only on gold NPs, i.e. on very dense particles. Dynamic light scattering (DLS) and nanoparticle tracking analysis (NTA) [19,20] are good al-

* Corresponding authors.

Email addresses: catia.contado@unife.it (C. Contado); luigi.calzolai@ec.europa.eu (L. Calzolai)

ternative candidate to estimate the amount of Igs by measuring the variation of particle diameter. Very recently, the increase in hydrodynamic radius of inorganic NPs was determined by fluorescence correlation spectroscopy (FCS), a technique suitable for in situ measurements [22]. The average number of proteins adsorbed on gold nanoparticles was recently determined also by combining two separation techniques, CPS and asymmetrical field flow fractionation (AF4) online coupled to a DLS detector [23].

The aim of this study differs from the previous ones since it seeks to compare the capabilities of the two separation techniques (both based on the centrifugal sedimentation, CPS and CF3) to measure the amount of aIgE adsorbed and to identify the formation of aggregates during the experiments. In fact, the aIgE adsorption onto the particle surface determines not only a mass (and size) increase but it could also promote the particle aggregation, as well known in the colorimetric biosensors field where the protein-induced aggregation of metal NPs is the requirement for the detection [24]. In addition, since it is highly possible to exceed the monolayer filling, leading to multilayer immobilization [25], these techniques can be used to verify if the aIgE-IgE reactivity is retained.

Two commercial samples of polystyrene beads of approximately 100 nm and 200 nm are used as a support and the aIgE and IgE are chosen for their role in the allergic reactions.

Firstly, the sizes of the initial substrates and their size variations due to the protein adsorption will be evaluated by DLS, CPS and CF3. Both CF3 (known in the past literature as sedimentation field flow fractionation, SdFFF) [26] and CPS sort the sample components depending on their buoyant mass [27,28], so that the parameters experimentally measurable, the retention time and the sedimentation time, depend on both size and density. The strength of CPS is the resolution while for CF3 is the possibility of being coupled online with a series of specific detectors, including DLS to monitor the separation. Online DLS measures the hydrodynamic diameter of the particles during their separation so that size and density can be deconvolved from the buoyant mass. Scanning electron microscopy (SEM) observations will be made to visually check the particles.

Secondly, the mass of aIgE adsorbed onto PS particles will be evaluated from the CF3 separations [15] while CPS measurements will provide a particle mass under the assumption that the particles be homogeneous. By merging the information acquired from the two techniques, the number of aIgE adsorbed on the PS particles will be evaluate from the mass data.

Finally, the anti-IgE-functionalized PS particles will be used to capture IgE molecules. The reaction will be followed by measuring the mass increase with CF3 and CPS. The particle aggregation induced by the aIgE and the IgE adsorption should be well identifiable from the elugrams of both techniques.

2. Theory

CF3 and CPS are both separation techniques based on the application of a centrifugal field [26,28], which sorts the sample components depending on their buoyant mass. The retention time and the sedimentation time, respectively, are so related to a physical parameter, which links size and density. Changing the density of the fluids in which the particles are separated, through a series of experiments, both CF3 and CPS allow the determination of the particle density provided the particles be homogeneous [29–31].

The creation of core-shell particles, as occurs when the PS particles come in contact with aIgE and IgE molecules, complicates the evaluation of the average particle size or the particle size distribution,

since the adsorbed molecules have usually a different density respect to the core.

The principles of the differential FFF [14–17,32–34] and some details regarding the CPS procedure [35,36] are reported in the Supplementary material (§ S.1), here in the following, only the relevant equations are recalled.

To measure the adsorbed mass $m_{c\,CF3}$ onto a spherical particle, the FFF differential procedure requires the measuring of the retention time of both uncoated (PS) and coated particles (PS-aIgE or PS-aIgE-IgE) through two independent CF3 analyses, performed under the same experimental conditions:

$$m_{c\,CF3} = \frac{kT}{Gw\left(1 - \frac{\rho_f}{\rho_c}\right)} \left[\frac{1}{\lambda_{p+c}} - \frac{1}{\lambda_p}\right] \tag{1}$$

where k is the Boltzmann's constant, T the absolute temperature during elution, w is the channel thickness, G the external field, ρ_f the fluid density, ρ_c is the density of the coating material, λ_p, and λ_{p+c} are the retention parameters referred to the bare (p) and the coated particle ($p+c$).

The adimensional parameter λ [26], under high retention conditions, i.e. $\lambda < 0.01$, is directly proportional to the retention ratio R

$$R = \frac{t_0}{t_r} \cong 6\lambda \tag{2}$$

Consequently, the amount reported in square bracket (Eq. (1)) is directly proportional to the shift in the retention times of the peak [15–17,32–34].

The CPS theory states that the time required by a spherical particle to sediment in the density gradient is [27,28]

$$t = \frac{18\eta ln\left(\frac{D}{S}\right)}{\left(\rho_p - \rho_f\right)\omega^2 d_p^2} \tag{3}$$

where d_p is the Stokes diameter of the particle settled and detected after time t, η is the dynamic viscosity of the fluid, D and S are respectively the ending (detection) and starting (start, inner liquid ring surface) radii of rotation, ρ_p and ρ_f are respectively the particle and liquid (fluid) density and ω is the angular frequency (radiant s^{-1}) of the disc.

When PS particles are coated with a layer of aIgE (or aIgE-IgE) the sedimentation time increases depending on the adsorbed mass. If the thickness of the layer is labeled d_c, the coated particle will have a total size $d_p = d_{PS} + 2d_c$ and a density equal to the sum of the core (PS) and shell masses divided by the particle volume

$$\rho_p = \frac{m_p}{V_p} = \frac{\rho_{PS}V_{PS} + \rho_c V_c}{V_p} \tag{4}$$

The amount experimentally measurable will be

$$\left(\rho_p - \rho_f\right) d_p^2 = \left(\rho_c - \rho_f\right)\left(d_{PS} + 2d_c\right)^2 + \frac{\left(\rho_{PS} - \rho_c\right) d_{PS}^3}{\left(d_{PS} + 2d_c\right)} \tag{5}$$

from which d_p, d_c and ρ_c can be determined only through complex

procedures [37–39] unless to have supplementary information about the protein thickness.

3. Materials and methods

3.1. Chemicals and reagents

Monodispersed polystyrene (PS) latex standards with nominal diameters of 100 nm and 196 nm, hereafter respectively indicated as PS100 and PS196, were purchased from G.Kisker GbR (PPS-0.1 and PPS-0.2, plain, 25 mg mL^{-1}, G.Kisker GbR Produkte f.d.Biotechnologie, Steinfurt, Germany); the amorphous density of the particles was assumed to be 1.050 g cm^{-3} [40].

aIgE (Goat anti human immunoglobulin E IgE Fc specific #G5G41-048 lot 17L33751 from Merdian Life Science, Inc. – Tebu-Bio Italy, Magenta (MI), Italy) and IgE (human IgE from Fitzgerald Industries International Inc., Concord MA, USA), were used to functionalize the PS particles. The assumed aIgE and IgE molecular weights were 150 kDa and 190 kDa [41], respectively, while the hydrodynamic diameters (top-to-bottom distance) were 14 nm (aIgE) [42,43] and 18 nm for the IgE [41]. The density was assumed to be 1.353 g cm^{-3} for both aIgE and IgE [43].

Table 1

Reagent volumes used for the preparation of the PS-aIgE binary systems and final concentrations. The number of PS particles and aIgE molecules and their ratio were theoretically computed from the concentration data. The suspensions were prepared in order to have the same (number of aIgE/total surface) ratio* between the 100 nm and 196 nm preparations. See §4.2.

	100 nm PS			196 nm PS		
aIgE coating preparation	1st	2nd	3rd	1st	2nd	3rd
Vol PB (pH=8, 10 mM) (μL)	450	420	390	465	450	435
Vol aIgE – 2.0 mg mL^{-1} (μL)	30	60	90	15	30	45
Vol PS – 2.5% g mL^{-1} – (μL)	20	20	20	20	20	20
Conc PS (% w v^{-1})	0.1	0.1	0.1	0.1	0.1	0.1
number of PS particles × 10^{10}	11.4	11.4	11.4	1.42	1.42	1.42
Conc aIgE (mg mL^{-1})	0.12	0.24	0.36	0.06	0.12	0.18
number of aIgE (×10^{17})	4.82	9.63	14.45	2.41	4.82	7.23
number of aIgE available for 1 PS particle (×10^{6})	4.24	8.48	12.7	16.95	33.90	50.86
Total PS surface (cm^2)	143	143	143	71.4	71.4	71.4
*number of aIgE/total surface (×10^{15})	3.37	6.74	10.1	3.37	6.74	10.1

The CF3 analyses were performed in phosphate buffer (PB), prepared by mixing 6.8 mL of NaH$_2$PO$_4$ 1 M and 93.2 mL of Na$_2$HPO$_4$ 1 M (Sigma Aldrich, Milan, Italy) to get pH 8.00. The measured density of the solvent, after the dilution to 10.0 mM with MilliQ water, at 24 °C was 0.9973 g cm^{-3}.

Ultrapure deionized water (MilliQ system from Millipore) was used to make all the solutions.

3.2. Adsorption of aIgE on PS particles

The procedure refers to the "1st preparation" of the PS100-aIgE sample (Table 1); all the other different PS-aIgE suspensions were prepared following the same protocol by changing only the volumes.

In a Protein LoBind Eppendorf-type tube 450 μL of the PB (pH 8.00, 10 mM) were mixed with 30 μL of the aIgE solution (2.0 mg mL^{-1}); the tube was vortexed at 500 rpm for one minute. 20 μL of polystyrene latex suspension (2.5% w/v) were added to the solution and the tube was vortexed for three minutes. The suspension was incubated for four hours on a constant end-over-end shaking at room temperature. After the adsorption process, to remove the excess of unbound protein, the coated latex particles were centrifuged at 13,200 rpm for 60 min (25 min for the PS196) (Eppendorf Microfuge 5415R, Brinkmann Instruments, Inc., Westbury, NY, USA) and 380 μL of the supernatant solution were replaced with an equal amount of a pure buffer solution. This cleaning procedure was repeated five times. The final concentration of the complex suspension, referred to the PS particles, was 0.1% w/v (Table 1 for all concentrations). The suspension was usually vortexed at 500 rpm for about 3–4 min before its analysis.

3.3. Antibody-antigen complex (PS-aIgE-IgE)

The procedure describes the preparation of the 1st ternary system PS100-aIgE-IgE (Table 2). All the other suspensions were prepared following the same protocol but using different volumes.

In a Protein LoBind Eppendorf-type tube 21.5 μL of the PB (pH 8.00, 10 mM) were mixed with 25 μL of the PS-aIgE suspension (0.1% w/v in terms of PS); the tube was vortexed at 500 rpm for 1 min and ultrasonicated for 1 min. Immediately after, 3.5 μL of a solution of human IgE (IgE =0.925 mg mL^{-1}) were added and the mixture, which was vortexed for 1 min and ultrasonicated in a bath for 30 s.

The suspension was incubated for one hour on a constant end-over-end shaking at room temperature. The achieved suspension was suitable for the analyses prior mechanical mixing with the vortex for about 3–4 min at 500 rpm.

Table 2

Reagent volumes for the preparation of the PS-aIgE-IgE ternary systems and final PS and IgE concentrations. The number of aIgE and IgE molecules and their ratio were computed from the theoretical concentration data.

	PS100-aIgE (100 nm PS)				PS196-aIgE 196 nm PS			
IgE coating preparation	1st	1st	2nd[a]	2nd satur	1st	1st	2nd[a]	2nd satur
Vol PB (pH=8, 10 mM) (μL)	21.5	24.0	34.6	12.0	7.0	27.0	15.0	31.0
Vol PS – aIgE (μL)	25.0	20.0	12.0	17.0	40.0	20.0	15.0	10.0
Vol IgE −925 μg mL^{-1} (μL)	3.5	6.0	3.4	21.0	3.0	3.0	2.0	9.0
Conc PS (%w v^{-1})	0.050	0.040	0.024	0.024	0.080	0.040	0.047	0.020
Conc aIgE (μg mL^{-1})	64.8	48.0	57.6	57.6	48.0	24.0	56.2	24.0
Conc IgE (μg mL^{-1})	64.7	111.0	62.9	388.5	55.5	55.5	57.8	166.5
IgE– aIgE ratio	1	2	1	7	1	2	1	7

[a] Not analysed.

3.4. Centrifugal field-flow fractionation (CF3)

A Postnova CF3 centrifugal Field Flow Fractionation system (model CF2000 Centri, Postnova Analytics GmbH, Landsberg am Lech, Germany) equipped with an UV–vis absorbance detector and online connected to a Malvern Zetasizer Nano-ZS instrument (Malvern Panalytical Ltd, Malvern, UK) detector was used to realize FFF-UV–vis-DLS measurements. The CF3 channel was 0.0229 cm thick, 57.6 cm long and 2.0 cm wide. The radius of the channel rotor was 10.015 cm. The channel void volume, declared in the instrument certificate, was 2.5087 mL. The carrier flow rate (PB phosphate buffer at pH 8.00, assumed viscosity 0.01 cp) was set to 1.0 mL min^{-1} and the UV–vis detection was recorded at 254 nm. The control of the CF3 system and the data collection/processing was performed by a personal computer equipped with the Postnova Analysis Software v2.05. All samples, vortexed for about 3–4 min before the analysis, were injected through a Rheodyne injector equipped with a 21.6 μL sample loop. The samples were let to equilibrate by stopping the carrier flow for 10 min (relaxation time) before starting the elution step.

The separations were performed at constant field, by setting the rotor velocity to 4800 and 2000 rpm respectively for the PS100 and PS196 samples; the correspondent gravities are 2582 g and 448 g (G/980 cm s^{-2}). All experiments were performed in duplicate at room temperature.

3.5. Centrifugal particle sedimentation (CPS)

A disc centrifuge instrument (Model DC24000, CPS instruments Inc., Prairieville, LA, USA), equipped with a 405 nm laser for the detection and running at 22,000 rpm was used to perform the CPS analysis. The sucrose (Sigma-Aldrich, Milan, Italy) density gradient 0%–8% (w/w) (nine different solutions of 1.6 mL in the range 0%–8% sucrose w/w in Milli-Q water) of nominal density 1.015 g cm^{-3}, was built within the disc rotating at 22,000 rpm and protected by a thin layer of 0.5 mL dodecane (Sigma-Aldrich, Milan, Italy). Once the equilibrium was set, the instrument was calibrated using poly(vinyl chloride) PVC standard particles (0.237 μm, CPS Analytik Ltd., Cambridge, UK; particle density 1.385 g cm^{-3}); this operation was repeated before each measurement. For the polystyrene particles a refractive index value of 1.624, absorption of 0.001 and density of 1.050 g cm^{-3} were used as input parameters for the calculations. The reproducibility was ensured collecting a minimum of three concordant measurements per sample.

3.6. Dynamic light scattering (DLS)

Dynamic light scattering measurements were performed on a Zetasizer Nano ZS (Malvern Instruments Ltd., Malvern, UK) equipped with a max 4 mW He–Ne laser, emitting at 633 nm, scattered light was measured in backscattering mode at 173° angle from incident beam. Samples were diluted as appropriate in the solvent (10 mM PB at pH 8) and equilibrated for 3 min before the measurements at 25 °C performed in disposable cuvettes. Size distribution results were generated by averaging 3 consecutive measurements of 12 times 10 s runs. A refractive index value of 1.590 and absorption of 0.01 were considered during the calculation of number based size distributions.

For CF3-DLS measurement the CF3 was linked to the same Zetasizer Nano ZS instrument using a quartz flow through cell with a light path of 3 × 3 mm (Hellma Optik GmbH Jena, Jena, Germany).

3.7. Zeta potential measurements

The zeta potential was measured by means of Zetasizer Nano ZS (Malvern Instruments Ltd., Malvern, UK) above described. The surface zeta potential was measured in disposable folded capillary cells (DTS1070, Malvern Instruments Ltd., UK) in 10 mM phosphate buffer (pH 8) after 1 min of temperature equilibration using automatic measurement duration, voltage and attenuation selection. Measurements were carried out in triplicates with 2 min delay between runs.

3.8. Scanning electron microscopy (SEM)

Particles were observed by using a Zeiss EVO 40 XVP (Carl Zeiss Microscopy GmbH, Jena, Germany) scanning electron microscope equipped with an Inca Energy 300 Oxford Instruments (Oxford Instruments NanoAnalysis, Wiesbaden, Germany) energy dispersive X-ray spectrometer (EDS) at an accelerating voltage of 20 kV. The samples were sputter coated under vacuum with a thin layer (20–30 Å) of gold.

4. Results and discussion

4.1. Characterization of the bare PS particles

In order to correctly interpret the results of surface coating, a good characterization of the PS particle, as they are available from the supplier, is of fundamental importance. 0.1% w/v suspensions were prepared from the commercial samples using as dilution media a PB at pH 8. The suspensions were manually shaken and then sonicated for 15 min before measuring their zeta potential, abundantly negative. The values, $\zeta = -62$ mV and $\zeta = -75$ mV observed in dilutions in the mobile phase (10 mM PB, pH8) respectively for the PS100 and PS196, were assumed as an indication of stable suspensions, which should preserve them from aggregation phenomena during their analysis. These negative values, however, do not exclude the presence of aggregates previously formed, demonstrable only by some sizing techniques.

Size information achieved with several independent techniques, DLS, CF3-DLS, CPS, are summarized in Table 3, while SEM pictures, taken to the batch samples, are reported in Fig. 1(a and b).

Table 3
Zeta potential and size information data for the PS bare particles. The ζ-potential values are the average of 3 measurements. DLS data were obtained on the batch suspensions (average of 4 measurements), CF3-DLS data refer to the DLS measurement done on-line during the CF3 separation. For the CF3 and CPS data, the assumed density was $\rho_p = 1.050$ g cm^{-3} [40]. The measured density of the PB at 24 °C was $\rho_l = 0.9973$ g cm^{-3}. The peak fitting was performed with Origin™ (Gaussian model). x_c and σ are the center and the standard deviation of the peak, respectively.

|	100 nm PS	196 nm PS
Zeta potential ζ (mV)	−61.9±11.6	−74.5±8.0
Sizes		
Supplier (nm)	100	196
DLS (Z-average) (nm), PdI	95.50, 0.02	199.18, 0.02
DLS (nm) Intensity - $x_c \pm$ RDS%	99.7±22.3%	206.7±21.4%
DLS (nm) Volume - $x_c \pm$ RDS%	89.9±25.1%	207.7±24.1%
Retention time 1st peak CF3[1] $x_c \pm \sigma$ (min)	12.95±3.21	16.49±3.23
CF3 (nm) – $x_c \pm \sigma$ 1st peak	91±6	181±10
CF3 (nm) – $x_c \pm \sigma$ 2nd peak (dimers)	112±6	219±23
CF3-DLS (nm) $x_{average} \pm st.dev$	104±8	196±5
CPS (nm) – $x_c \pm \sigma$ 1st peak	93±5	182±4
CPS (nm) – $x_c \pm \sigma$ 2nd peak (dimers)	112±3	219±4
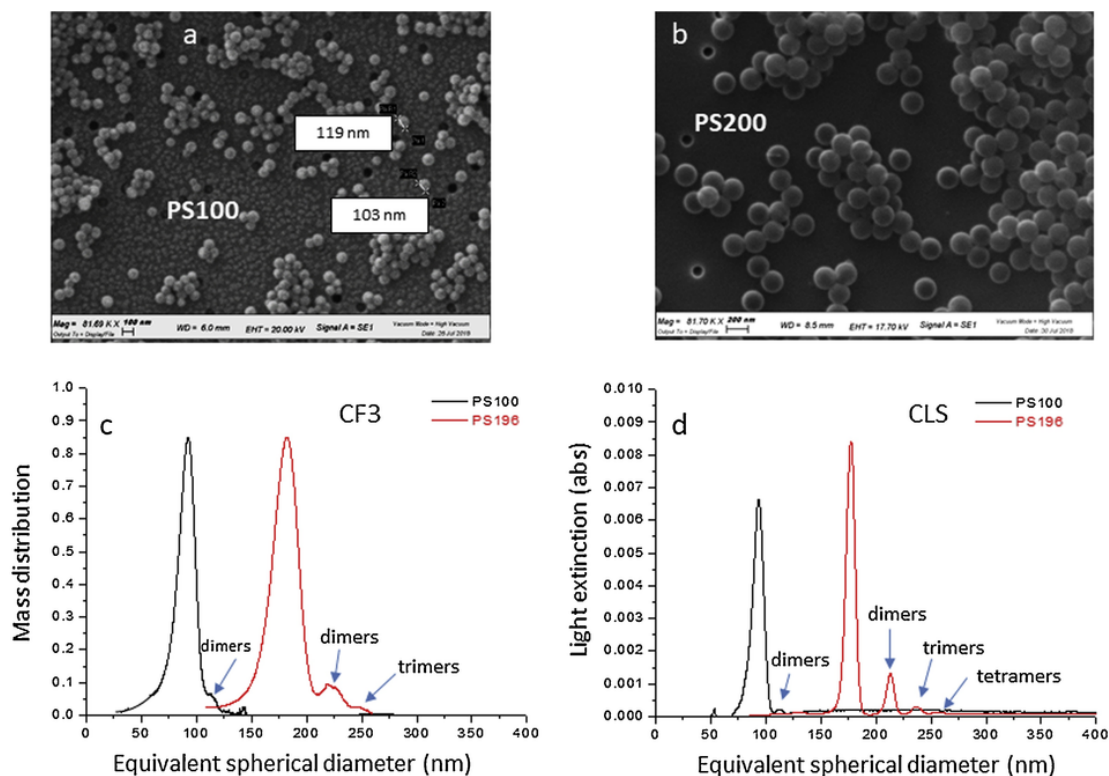
Fig. 1. SEM pictures of the 100 nm (a) and 196 nm (b) polystyrene samples; magnification 82 K. Particle size distributions of the PS particles obtained from the (**c**) CF3 and (d) CPS separations. Experimental conditions: (**c**) 21.6 µL injection volume, carrier PB at pH 8.00, flow rate 1 mL min^{-1}, centrifugal fields 4800 rpm (PS100) and 2000 rpm (PS196); (d) injection volume 0.4 mL, 0%–8% w/w sucrose gradient, centrifugal speed 22,000 rpm.

Batch mode DLS was firstly applied as fast and simple method to check the compliance of the particle sizes with that declared by the producer. Measured diameters were in reasonable agreement with the declared values, even if they tended to be smaller in the case of the PS100 sample and higher for the PS196.

In order to verify if the commercial samples were really monodispersed suspensions, particle size distributions were also derived from CF3-UV-DLS and CPS measurements, by taking advantage of the great separation abilities of these two techniques, both based on the action of a centrifugal field. Since the particles are sorted depending on their buoyancy mass, to convert the mass information into size values the particle density should be known; in these experiments a value of 1.050 g cm^{-3} was used for both PS samples.

The CF3 mass distributions (Fig. 1c) show for both PS100 and PS196 samples two peaks, whose sizes, expressed as equivalent spherical diameter, were respectively 93 nm and 181 nm for the main, largest peaks, and 112 nm and 219 nm for the secondary small peaks, indicated on the figure with blue arrows (dimers, see also Table 3).

These bimodal distributions were detected also by the CPS (Fig. 1d), and the sizes correspondent to those peaks were 93 nm and 112 nm for the PS100 sample, and 182 nm and 218 nm for the PS196 sample. These first results obtained with the two independent techniques were surprisingly very consistent with each other.

To verify if the small, secondary peaks are due to dimers and trimers, the apparent Stokes diameters of the multiples were computed with the empirical relation reported by Mehn in Ref. [44] and firstly suggested by Bondoc and Fitzpatrick [45]

$$d_{app,N} = \left(0.518 + 0481 N^{0.5}\right) d_{app,1} \tag{6}$$

The computed values with this relation, which holds true for small aggregates ($N \leq 6$), differed from the CF3 experimental data of -3% (PS100) and -1% (PS196) and less than 1% for the separations performed with the CPS (see Table S1 in Supplementary Material). These results were considered an indirect confirmation of the hypothesis that both diluted samples contain a small percentage of dimers, and that the PS196 nm sample contained also trimers and tetramers.

By taking advantage of the CF3-UV-DLS instrumental configuration, the CF3 separations were monitored also by the DLS, which gives an independent size measurement of the separated particles, allowing to verify the veracity of the assumed PS density. The sizes measured online with the DLS in correspondence of the main peaks were 104 nm and 196 nm respectively for the PS100 and PS196 (Table 3 – CF3-DLS data). These numbers, taken as the most reliable, if inserted in Eq. (S4), allow to evaluate from the measured mass value m_{PS}, the density. When the particle density was adjusted to 1.038 g cm^{-3} (Eq. (S4)) [14,15,26], the sizes determined by converting the retention times matched the DLS data for both PS samples.

In an attempt to cross-validate this result through the CPS experiments, this density was used to re-calculate the particle sizes. The new values of the equivalent spherical diameters were higher than those previously computed (with $\rho_p = 1.050$ g cm^{-3}); they were 110 nm and 214 nm, respectively (Table S1); to match the sizes computed by CF3-DLS the density had to be set to 1.045 g cm^{-3}.

Since the two techniques did not converge to an unique density value, in the following experiments, when required, the nominal value of 1.050 g cm^3 was used as density of the core particles.

4.2. Characterization of the PS-aIgE binary systems

The suspensions of the PS-aIgE binary systems were prepared for both PS100 and PS196 samples in order to get 0.1% w/v PS particles in all final preparations, while the concentration of aIgE was proportional increased from the first to the third preparation (for example, for the PS100, 0.12, 0.24, 0.36 mg mL^{-1}) and set to have an equal nominal number of aIgE molecules for PS surface unit for correspondent preparations, i.e. the 1st preparation had $\approx 3.4 \times 10^{15}$ aIgE molecules cm^{-2} for both PS100 and PS196 samples (Table 1, last row).

The adsorption of the aIgE onto the particle surface determined a significant decrease in the zeta potential in all preparations, which was leveled out at roughly $\zeta \approx -20$ mV (Table 4). The first preparation showed a slightly lower ζ value for both PS samples ($\zeta = -23$ mV PS100 and $\zeta = -25$ mV PS196), compared to the second and the third preparation, for which the ζ values were very similar ($\zeta = -20$ mV, PS100 and $\zeta = -19$ mV, PS196). This trend was taken as an indirect indication of having reached a saturation condition on the surface, which could be "geometrical" or physical, since the electrostatic interaction between the protein coating on the surface and the protein molecules in solution might hinder the adsorption of further molecules.

Fig. 2 shows the CF3 elugrams of the PS and PS-aIgE particles for the PS100 (plot a) and PS196 (plot b) samples; the retention time shift of the main peaks due to the mass increase is evident in both plots. The decrease of the UV signal of the PS-aIgE binary systems respect to the PS particles can be ascribed to the screen effect of the adsorbed aIgE on the PS surface, which reduces the PS adsorption at 254 nm and to the re-distribution of the particles in multiplets. The increased amount of aggregates can be deduced by either the area increase of the secondary peaks and the appearance of a strong signal when the centrifugal field stops (data not shown on the elugrams). The aIgE molecules can favor the aggregation making bridges among the particles and by lowering the surface potential (Table 4, ζ values); this latter effect could provoke also a particle loss due to irreversible interactions of the PS-aIgE particles with the channel walls, especially that one toward which the particles are pushed by the centrifugal field.

These evidences were confirmed also by the CPS graphs depicted in Fig. 3, where the light extinction (absorption and scattering based signal loss) is reported as a function of the equivalent spherical diameter, computed by the software by comparing the sedimentation behavior of the samples with the PVC standard particles of 0.237 nm. The signal of the bare particles was scaled respect to the peak height of 10 times (plot a) and 20 times (plot b), respectively. The aggrega-

Table 4
Zeta potential, mass and size information data for the PS-aIgE binary systems. The zeta potential values are the average of 3 measurements. Mass of the coating $m_{c\,CF3}$ (Eq. (1)): assumed densities $\rho_{PS} = 1.050$ g cm^{-3} (PS) [40], $\rho_c = 1.353$ g cm^{-3} (aIgE) [43]; measured density of the PB $\rho_l = 0.9973$ g cm^{-3}. CF3-DLS data refer to the DLS measurement done online during the CF3 separation. The peak fitting was performed with Origin™ in order to obtain the peak center (x_c) and the standard deviation σ of the peak (1: Gaussian model; 2: Gaussian modified model).

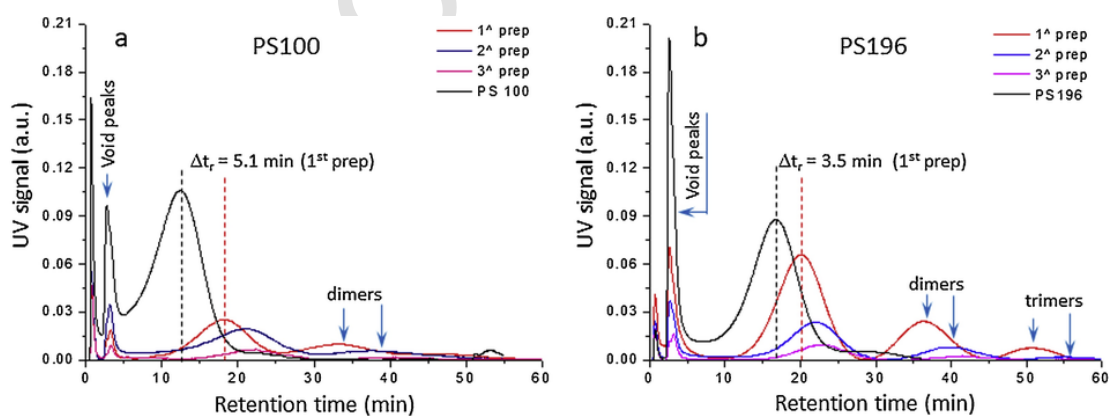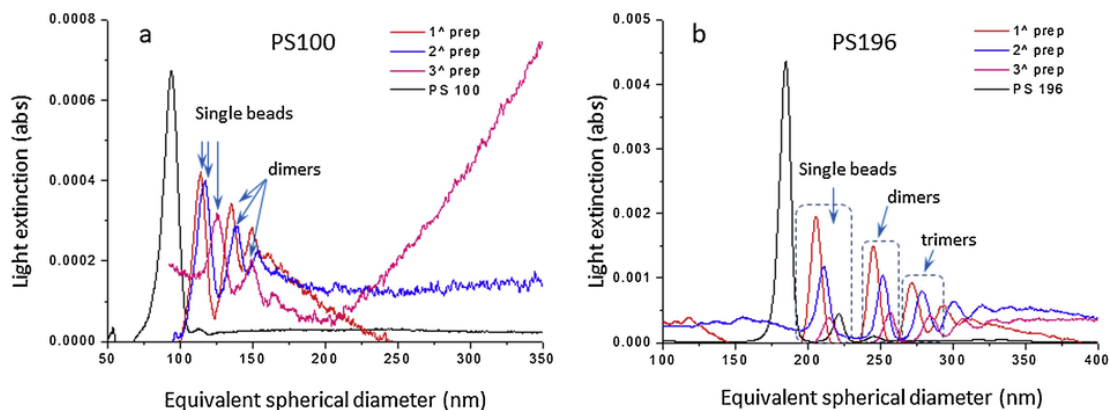| 1		100 nm PS			196 nm PS		
2	PS-aIgE preparation	1st	2nd	3rd	1st	2nd	3rd
3	Zeta potential ζ (mV)	-23.2 ± 5.2	-18.5 ± 4.0	-20.7 ± 4.5	-24.9 ± 4.4	-19.2 ± 4.4	-18.8 ± 3.9
4							
5	Retention time t_r CF3^1 1st peak (min) $x_c \pm \sigma$	18.0 ± 3.0	20.6 ± 3.9	21.9 ± 3.5	20.0 ± 2.9	21.9 ± 3.0	22.8 ± 3.1
6	CF3 Δt_r (min)	5.10	7.67	8.95	3.48	5.38	6.27
7	$m_{c\,CF3}$ (g × 10^{-17}) Eq. (1)	3.31	4.97	5.80	12.98	20.06	23.40
8	CF3-DLS 1st peak (nm) $x_{average} \pm st.dev$	114 ± 5	121 ± 8	139 ± 17	213 ± 7	221 ± 9	232 ± 18
9	CF3-DLS 2nd peak (nm) $x_{average} \pm st.dev$	143 ± 7	150 ± 14	170 ± 26	251 ± 12	269 ± 16	Not measurable
10	CF3-DLS 3rd peak (nm) $x_{average} \pm st.dev$	Not measurable	Not measurable	Not measurable	294 ± 16	345 ± 35	Not measurable
11	Radius of the coating (nm)	7	10	18	8	13	18
12	CPS^2 1st peak (nm) $x_c \pm \sigma$	113 ± 4	116 ± 4	125 ± 4	205 ± 4	211 ± 4	216 ± 4
13	CPS^1 2nd peak (nm) $x_c \pm \sigma$	132 ± 5	138 ± 4	148 ± 5	245 ± 4	252 ± 4	258 ± 4
14	CPS^1 3rd peak (nm) $x_c \pm \sigma$	149 ± 2	153 ± 4	Not measurable	272 ± 5	280 ± 5	286 ± 5
15	CPS^1 4th peak (nm) $x_c \pm \sigma$	Not measurable	Not measurable	Not measurable	294 ± 5	302 ± 8	310 ± 10
16	ρ_c (g cm^{-3}) - Eq. (S29)	1.046	1.024	1.022	1.034	1.035	0.9963
17	$m_{c\,CPS}$ (g × 10^{-16})	2.01	3.44	8.32	11.6	18.3	26.1

Fig. 2. Superimposed CF3 elugrams of the PS particles and PS-aIgE binary systems monitored with the on-line UV detector, set to 254 nm; separations performed with a flow rate of 1 mL min^{-1}, centrifugal fields 4800 rpm (a) and 2000 rpm (b) for the PS100 and PS196 samples, respectively.

Fig. 3. Graphs reporting the light extinction as a function of the equivalent spherical diameter obtained from the CPS separations performed in a 0%–8% w/w sucrose gradient with a centrifugal speed of 22,000 rpm; (a) PS100 and (b) PS196 samples.

tion among particles induced by the aIgE molecules was proven for both PS samples by the appearance of large and broad peaks during the separations of the second and third preparations (Fig. S3), in the range 200–1000 nm for the PS100 and between 300 and 500 nm for the PS196.

The mass of the adsorbed layer $m_{c\,CF3}$ can be determined with Eq. (1) [14,15], providing a number of assumptions are made, on the top of which to attribute the retention time shifts only to the particle mass variation, neglecting the retardation caused by possible interactions of the particles with the channel walls, which would deviate the elution behavior from the ideal case. This assumption, reasonably for the bare PS particles, is more challenging for the PS-aIgE binary systems.

To avoid interactions between bare and coated particles, the separations were carried out in separate runs, maintaining the same experimental conditions. The mass coating $m_{c\,CF3}$ was firstly computed from the retention time differences of the main peaks by assuming as known the density of the coating material ρ_c.

Coatings of the order of 10^{-17} g/particle were obtained in all experiments (Table 4), with an average increment of $\approx 34\%$ between the first and the second preparation, and only of the 14% between the second and the third. By assuming a Mw of 150 kDa for the aIgE [7], the $m_{c\,CF3}$ adsorbed correspond to roughly 130 up to 230 molecules/particle for thePS100, and 520 up to 940 molecules/particle for the PS196 (Table 5, row 7). These numbers are significantly smaller than the theoretical number of molecules available in solution for a single particle (N), however, the ratios $\theta_{exp\text{-}CF3}/N$ for corresponding preparations are very similar (~ 3.0 - 1st prep, ~ 2.4 - 2nd and ~ 1.8 - 3rd). This means that the PS particles, PS100 and PS196, captured a number of aIgE proportional to the concentration of the molecules in suspensions, but independently of the size of the PS sphere.

A similar conclusion could be deduced by observing the mass of aIgE adsorbed ($m_{c\,CF3}$) related to the particle surface; values of coating ranging between ˜0.26 and ˜0.46 mg m^{-2} are found, in agreement with the results achieved by adsorbing IgG on PS microparticles (Table 5, row 6) [9].

Table 5

Comparison between the experimental and the theoretical data for the PS-aIgE binary systems. θ measures the number of aIgE adsorbed on a single PS particle, computed from $m_{c\,CF3}$ or $m_{c\,CPS}$ data and by assuming a Mw of 150 kDa. N measures the number of aIgE available in solution for each single PS particle. The surface of the circle occupied by an aIgE ($R_h = 6.50$ nm) is 1.33×10^{-12} cm^2. *$m_{c\,CF3}$ was computed with Eq. (1) by using the ρ_c values computed through Eq. (S29) (Supplementary material).

1		100 nm PS			196 nm PS		
2	Surface area of the sphere cm^2 ($\times 10^{-9}$)	1.26			4.83		
3	Theoretical number of aIgE adsorbable (packing type)	859 (hexagonal)		744 (square)	3299 (hexagonal)		2857 (square)
4	PS-aIgE preparation	1st	2nd	3rd	1st	2nd	3rd
5	CF3 data						
6	$m_{c\,CF3}$/particle surface (mg m^{-2})	0.25	0.38	0.45	0.27	0.41	0.48
7	$\theta_{exp\text{-}CF3}$	127	194	227	521	805	939
8	N $\times 10^6$	4.24	8.48	12.7	16.95	33.90	50.86
9	$\theta_{exp\text{-}CF3}/N$ ($\times 10^{-5}$)	3.0	2.3	1.8	3.1	2.4	1.8
10	Percentage of coverage/particle (exagonal packing)	15	23	26	16	24	28
11	Percentage of coverage/particle (square packing)	17	26	31	18	28	33
12	*$m_{c\,CF3}$ (g $\times 10^{-16}$)	1.81	4.93	6.24	19.1	23.5	25.9
13	*$\theta_{exp\text{-}CF3}$	726	1979	2504	7653	9432	10398
14	*$\theta_{exp\text{-}CF3}/N$ ($\times 10^{-4}$)	1.71	2.33	1.97	4.51	2.79	2.04
15	*Percentage of coverage/particle (hexagonal packing)	84	230	291	232	286	315
16	*Percentage of coverage/particle (square packing)	98	266	337	268	330	364
17	CPS data						
18	$m_{c\,CPS}$ (g $\times 10^{-16}$) Eq. (7)	2.01	3.44	8.32	11.6	18.3	26.1
19	m_c/particle surface (mg m^{-2})	1.60	2.73	6.62	2.40	3.80	5.40
20	$\theta_{exp\text{-}CPS}$	806	1379	3339	4645	7358	10468
21	Percentage of coverage/particle (hexagonal packing)	93	160	388	141	223	317
22	Percentage of coverage/particle (square packing)	108	185	449	163	258	366

Since, none specific surface investigation were made to infer the orientation of the aIgE molecules on the surface, all possible arrangements are equally considered [47,48] even if, it is reasonable to suppose that they are likely adsorbed through the Fc hydrophobic fragment [49] because of the basic pH (PB, pH=8) of the solution; this hypothesis will be verified if the Ag-Ab reaction, foreseen as following step, occurs.

By assuming that the aIgE are macromolecules of hydrodynamic radius R_h =6.50 nm [42], the projected area of the circle that a single molecule can cover is 1.33×10^{-12} cm^2, no matter what its orientation as it approaches the surface. The ratio between the PS sphere surface and the circle hypothetically occupied by a molecule, multiplied by the packing density coefficient [50], gives the maximum number of aIgE that can cover a single bead (Table 5, row 3). The number of molecules adsorbed, expressed as percentage of coverage for the two packing geometries, hexagonal and square (rows 10 and 11), both indicate that the geometrically possible saturation condition is never reached, even if the ζ potential values do not vary between the 2nd and 3rd preparation.

Thanks to the online DLS detector, the sizes of the PS-aIgE particles were measured during their elution (Table 4 - CF3-DLS data, and Figs. S4–S5). The difference between these CF3-DLS data and those measured for the bare particles brings to an estimated layer thicknesses of 7 nm (PS100) and 8 nm (PS196), smaller than the aIgE top-to-bottom distance of 14 nm [42,48]. The layer thickness computed for the 3rd preparation was approximately of 18 nm (>14 nm) for both PS samples, a number that could suggest the presence of multiple aIgE layers. By merging this information with the presence of broad peaks observed in both CPS graphs (Fig. S3), the 3rd preparation was not considered for the subsequent Ag-Ab reaction.

The above considerations can be critically questioned by the following discussion. The mass of aIgE adsorbed onto the PS surface could be determined, in principle, also from the CPS experiments, even if the procedure is much more complex because density and sizes are both contemporaneously related to the core and the coating. However, in this study, it is possible to merge the CPS information with that obtained from the CF3-DLS to determine the density and the mass of the adsorbed aIgE layer. CPS analysis requires to input the particle density to obtain the particle size distribution; once the sizes are known, the mass measured by the CPS is easily back-calculable. This mass is due to the sum of the core and the aIgE shell. By assuming that the mass of the coated particle does not change when the particles are separated by CPS or CF3 (see also Supplementary material), the diameters determined by CF3-DLS can be used to complete the following equation

$$\left(\rho_{PS} - \rho_{sucrose}\right) \frac{\pi}{6} d_{CPS}^3 = \left(\rho_{PS} - \rho_c\right) \frac{\pi}{6} d_{CF3-DLS\,core}^3 + \left(\rho_c - \rho_{sucrose}\right) \frac{\pi}{6} d_{CF3-DLStot}^3 \quad (7)$$

where $\rho_{sucrose}$ is the average density of the sucrose solutions between the starting point of sedimentation and the detector position (1.015 g cm^3) [51]. This equation can be solved to obtain the density of the aIgE shell (ρ_c) (see Eq. (S29)) and consequently the mass of the shell ($m_{c\,CPS}$) (Table 4). All density values are <1.3 g cm^{-3}, as reported in literature for proteins; and also smaller than 1.06 g cm^{-3} as observed by J. Vörös [52], who studied the adsorption of IgG on Teflon surfaces. This result is due to the fact that the aIgE coating is not a closely packed layer, but it contains a significant amount of solvent, variable from a 30% [23] to 70% [53]. The values decrease as a func-

tion of the preparation and the smallest particles appear to have a slightly denser protein shell, in agreement with the trend observed by N.C. Bell et al. [14].

The mass of the coating ($m_{c\,CPS}$) computed by using these densities are of one order of magnitude greater than those previously computed by CF3 ($m_{c\,CF3}$) (cfr rows 7 and 17 Table 4), to which correspond a number of adsorbed molecules (θ_{exp} -$_{CPS}$) consequently higher (Table 5). The percentage of coverage are in almost all cases greater than 100% compared to the theoretical values, a result that could explain why the ζ potential was constant for 2nd and 3rd preparations.

In the light of these findings, also the $m_{c\,CF3}$ calculations (Eq. (1)) were revised by using the shell densities (ρ_c) determined for each preparation (Table 4, row 16). The new *$m_{c\,CF3}$ data (Table 5, row 12) are now in line with those computed by CPS, determining a number of aIgE adsorbed on a single PS particle (*$\theta_{exp-CF3}$) of the same order of magnitude of the $\theta_{exp-CPS}$ values; obviously, to different density values correspond different amount of water adsorbed in each layer, so that the correspondence between analogous preparation is lost (*$\theta_{exp-CF3}$/N). By concluding, the shell density reveals itself as the most critical parameter in the CF3 theory, which must be chosen, when possible, only after accurate and complementary measurements.

4.3. Characterization of the PS-aIgE-IgE ternary systems

The amount of IgE placed in contact with the PS-aIgE complex was established by setting to 1:1, 1:2 and 1:7 (large excess) the molecular ratio with the aIgE previously used to build the binary complex PS-aIgE. To test the behavior of the PS-aIgE probes and to compare their performance toward the aIgE-IgE reaction, the IgE concentration in the final suspensions was kept higher than the typical IgE concentration found in human sera of allergic patients (IgE=12 μg mL^{-1}, 5000 IUmL^{-1}) [54]; the values ranged between 65–390 μg mL^{-1} (PS100) and 55–166 μg mL^{-1} (PS196).

The Ag-Ab complex formation determines an increment of the particles' mass which both CF3 and CPS can monitor. Fig. 4 reports the PS100-aIgE elugram of the first preparation (Table 1) superimposed to the elugrams of the 1:1 and 1:2 ternary systems (Table 2, columns 2–3). The separation was monitored by both UV and DLS detectors but – in the actually used instrument setup - often only this latter gave a signal strong enough to clearly distinguish the peaks [14]. If the analysis time is fixed to one hour, this time interval allows to monitor the exit of the main peak, to measure the retention time shift and consequently the mass uptake. However, to verify the presence of aggregates, the CF3 analysis time would be much longer, without having the certain of obtaining a complete picture of the fractionated sample. These considerations brought us to prefer the CPS instead of the CF3.

Fig. 5 shows the separations of both PS100 (a) and PS196 (b) samples by CPS. Both graphs show a very broad roughly Gaussian curve, peaking at roughly 320 nm for both PS100-aIgE-IgE samples and 350 nm for both PS196-aIgE-IgE samples due to the agglomeration of the IgE and the particles. Superimposed to this broad curve, as observed by Gollwitzer et al. [55], a number of very narrow peaks are present on all the left sides of the large peaks, ascribable to well defined multiples (monomers, dimers, trimers, etc), as proven by the numerical data summarized in Table 6. These narrow peaks were better defined in the suspensions created with the 196 nm PS particles.

By considering that PS-aIgE-IgE complexes were created through independent experiments, the surprising match of the estimated sizes of the first, second, etc. peaks of the 1:1 and 1:2 preparations (columns 2–3 and 4–5), even if computed with an incorrect particle density, suggests a well defined ratio between aIgE and IgE molecules.
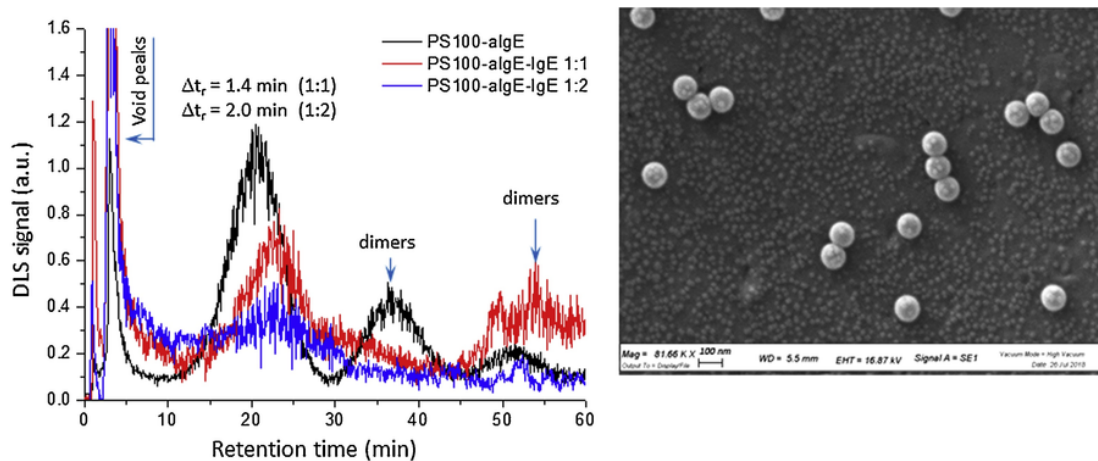
Fig. 4. CF3 elugrams of the 1st preparation of the PS100-aIgE binary system (black line) and the PS100-aIgE-IgE ternary systems prepared as reported in Table 2. The ratios 1:1 (red line) and 1:2 (blue line) are referred to the theoretical aIgE:IgE number of molecules. Separation monitored with the online DLS detector; laser light emitted at 633 nm; 21.6 μL injection volume, carrier PB at pH 8.00, flow rate 1 mL min^{-1}, centrifugal fields 4800 rpm. SEM picture of the PS100-aIgE binary system; magnification 82 K. For interpretation of the references to colour in this figure legend, the reader is referred to the web version of this article.)
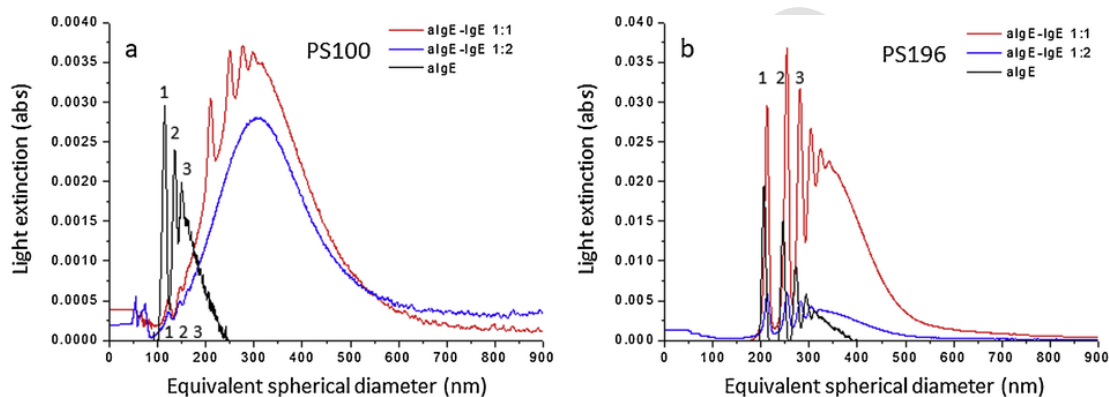
Fig. 5. Graphs reporting the light extiction as a function of the equivalent spherical diameter obtained from the CPS separations of the 1st preparation of the PS-aIgE binary system (black line) and the PS-aIgE-IgE ternary systems prepared as reported in Table 2. The ratios 1:1 (red line) and 1:2 (blue line) are referred to the theoretical aIgE:IgE number of molecules. Data obtained starting from the PS 100 nm (a) and PS 196 nm (b) samples, respectively. Separations performed in a 0%–8% w/w sucrose gradient and with a centrifugal speed of 22,000 rpm. The numbers 1, 2, 3 indicate the peaks due to single particles, dimers and trimers, respectively. For interpretation of the references to colour in this figure legend, the reader is referred to the web version of this article.)

The Ab-Ag reaction determined a size increment percentage of ≈ 8–9% and ≈ 3–4% for the 1:1 and 1:2 preparations respectively for the PS100 and PS196 samples.

The mass increment of the PS-aIgE particles, due to the capture of the IgE, is computable through the CF3 experiments, but the shift in the retention times Δt_r was well determinable only in the case of the PS196 samples. Since no experimental, reliable data for the densities of each single preparation were available, Eq. (1) was then solved by using for ρ_c the literature value ($\rho_c = 1.353$ gcm^{-3} [43]). The mass was calculated by comparing the retention data of the ternary systems respect to the PS bare particles and then subtracting the contribution due to the creation of the first layer (aIgE), computed always using the same density. The mass increment, Δm, is roughly of 1×10^{-16} g for the 1:1 and 1:2 preparations, and 1.3×10^{-16} g for the excess. The molecular ratio between the IgE and aIgE present on the surface, is roughly 0.6 in almost all cases (Table 6, row 18), which indicates that only half of the aIgE (Fc specific) adsorbed on the surface can interact with the IgE. Unfortunately, the lack of on-line CF3-DLS sizes (Z-average) limits any further consideration about the layer thickness, impeding to calculate the IgE shell density and the mass also from the CPS experiments. For a more accurate application of Eq. (1) and a

critical discussion of the CF3 method, a different experimental approach must be excogitated.

5. Conclusions

In this work, a careful size characterization of the PS particles, used as substrates for the protein adsorption, was carried out. The results obtained by comparing different sizing techniques (DLS, CPS and CF3) showed that sometimes samples sold as monodispersed might contain dimers or multiplets in small quantity. The accurate knowledge of the particle dimensions in case of homogeneous spheres allows the estimation of the particle density from the CF3 data, since this technique sorts the sample based on their mass. However, this value (1.038 gcm^{-3}) should be used with caution, since when used to back-calculate the diameters from the CPS experiments, the computed diameters resulted larger than expected. The correspondence between the sizes determined with independent techniques and those computed from the CPS experiments is found for a density of 1.045 gcm^{-3}, smaller but closer to the declared value. In both cases, the Stokes diameters were smaller than the hydrodynamic diameters measured by DLS.

Table 6

CLS and CF3 data of the PS 100-aIgE-IgE and PS 196-aIgE-IgE complexes. The CPS peak fitting was performed with Origin™ in order to obtain the peak center (x_c) and the standard deviation σ of the peak (1: Gaussian model, 2: Gaussian modified model). CF3 data were obtained by monitoring the elution with the online DLS. CF3-DLS data refer to the DLS measurement done online during the CF3 separation. Mass of the protein coating $m_{c\,CF3}$ (Eq. (1)): assumed densities $\rho_p = 1.050\,\mathrm{g\,cm^{-3}}$ (PS), $\rho_c = 1.353\,\mathrm{g\,cm^{-3}}$ (aIgE) [43]; measured density of the PB $\rho_l = 0.9973\,\mathrm{g\,cm^{-3}}$.

1		PS100-aIgE			PS196-aIgE		
2	CPS	1st		2nd	1st		2nd
3	CPS^2 1st peak (nm) $x_c \pm \sigma$	113±4		116±4	205±4		211±4
4	IgE/aIgE ratio	1:1	1:2	1:7 (excess)	1:1	1:2	1:7 (excess)
5	CPS^1 1st peak (nm) $x_c \pm \sigma$	122±5	122±4	131±6	212±4	212±5	227±4
6	Size increment %	8%	8%	13%	3%	3%	7%
7	CPS^1 2nd peak (nm) $x_c \pm \sigma$	147±8	146±20	158±4	253±4	253±5	272±4
8	Size increment %	9%	8%	14%	3%	3%	8%
9	CPS^1 3rd peak (nm) $x_c \pm \sigma$	210±5	163±15	176±9	281±6	282±6	303±6
10	Size increment %	40%	9%	15%	3%	4%	8%
11	CPS^1 4th peak (nm) $x_c \pm \sigma$	250±5	–	191±10	304±7	305±8	328±9
12	Size increment %	Not eval.		Not eval.	4%	4%	9%
	CF3	1st		2nd	1st		2nd
13	CF3 t_r 1st peak (min) PS-aIgE $x_c \pm \sigma$	18.0±3.0		20.6±3.9	20.0±2.9		21.9±3.0
	IgE/aIgE ratio	1:1	1:2	1:7 (excess)	1:1	1:2	1:7 (excess)
14	CF3 t_r 1st peak (min) PS-aIgE-IgE $x_c \pm \sigma$	Detector signal too weak	Detector signal too weak	Detector signal too weak	22.8±3.13	23.02±3.46	25.36±10.5
15	CF3 Δt_r (min)	–	–	–	6.31	6.53	8.87
16	$m_{c\,CF3}$ (g×10⁻¹⁷) Eq. (1).	–	–	–	23.52	24.34	33.06
17	Δm_{c-CF3} (g×10⁻¹⁶)	–	–	–	1.05	1.14	1.30
18	IgE/aIgE	–	–	–	0.6	0.7	0.5
19	CF3-DLS 1st peak (nm) $x_c \pm \sigma$		–		204±12.46	206±5.96	No well defined peak
20	CF3-DLS 2nd peak (nm) $x_c \pm \sigma$	–			–	251±9.24	No well defined peak

The same pool of techniques and the tested strategy were very useful also to study the adsorption of aIgE onto the PS particles, since this process determines an increase of the particle sizes and masses and promotes the aggregation among the particles. The mass of the adsorbed aIgE molecules can be directly measured through CF3 experiments, but the CPS, used in parallel, reveals being very useful in determining the density and the mass of the protein shell by combining its size data with those obtained by the coupling CF3-DLS. The masses of aIgE adsorbed onto the particles, computed by CF3 using the density reported in literature, were initially smaller than that calculated from the CPS and CF3-DLS data, but when the experimental ρ_c density values, calculated by merging the CPS and CF3-DLS data, were inserted in Eq. (1), the mass of aIgE adsorbed onto the PS particles became consistent with the CPS data and with the ζ-potential data.

When the functionalized PS particles were used to capture IgE molecules, both CF3 and CPS techniques detected a further mass increase, and the ratio between the primary and secondary antibodies inferred from the CF3 mass data foresees that only roughly half of adsorbed aIgE interact with an IgE molecule. However, the diffuse aggregation among molecules and particles, monitored very rapidly by the CPS, did not allow a stable UV signal and significant CF3-DLS size data for all the preparations to support more strongly these data. This could be avoided by washing the ternary complex, but the choice of leaving the PS-aIgE-IgE particles in the reaction medium was done thinking to the PS-aIgE particles as probes for capturing the IgE directly in biological fluids (serum). A new experimental approach must be thought to overcome the limits encountered in this work and it will be object of a future investigation. In addition, as it is difficult to distinguish the aggregation due to specific reaction with the allergen from the non-specific aggregation of particles, the application to detect allergies might require refinement of the protocol, i.e. the use of monoclonal or synthetic antibodies.

Uncited references

[46].

Appendix A. Supplementary data

Supplementary material related to this article can be found, in the online version, at doi:https://doi.org/10.1016/j.chroma.2019.460383.

References

[1] C.E. Giacomelli, Immunoglobulins: adsorption at solid–liquid interfaces, In: P. Somasundaran, A.T. Hubbard (Eds.), Encyclopedia of Surface and Colloid Science, vol. 1, Taylor & Francis, Boca Raton, Fl, 2006, pp. 510–530.

[2] E.L. Ng, E.H. Lwanga, S.M. Eldridge, P. Johnston, H.-W. Hu, V. Geissen, D. Chen, An overview of microplastic and nanoplastic pollution in agroecosystems, Sci. Total Environ. 627 (2018) 1377–1388, https://doi.org/10.1016/j.scitotenv.2018.01.341.

[3] C. Loos, T. Syrovets, A. Musyanovych, V. Mailänder, K. Landfester, G.U. Nienhaus, T. Simmet, Functionalized polystyrene nanoparticles as a platform for studying bio–nano interactions, Beilstein J. Nanotechnol. 5 (2014) 2403–2412, https://doi.org/10.3762/bjnano.5.250.eCollection 2014.

[4] M. Dabkowska, Z. Adamczyk, Mechanism of immonoglobulin G adsorption on mica-AFM and electrokinetic studies, Colloids Surf. B 118 (2014) 57–64, https://doi.org/10.1016/j.colsurfb.2014.02.053.

[5] C. Minelli, A. Sikora, R. Garcia-Diez, K. Sparnacci, C. Gollwitzer, M. Krumrey, A.G. Shard, Measuring the size and density of nanoparticles by centrifugal sedimentation and flotation, Anal. Methods 10 (2018) 1725–1732, https://doi.org/10.1039/C8AY00237A.

[6] J.M. Cruse, R.E. Lewis, Atlas of Immunology, third ed., CRC Press/Taylor & Francis, Boca Raton, Florida, 2010.

[7] I. Roitt, J. Brostoff, D. Male, Immunologia, fifth ed., Zanichelli, Bologna, 2003.

[8] R. Asero, B.K. Ballmer-Weber, K. Beyer, A. Conti, R. Dubakiene, M. Fernandez-Rivas, K. Hoffmann-Sommergruber, J. Lidholm, T. Mustakov, J.N.G. Oude Elberink, R.S.H. Pumphrey, P.S. Skov, R. van Ree, B.J. Vlieg-Boerstra, R. Hiller, J.O. Hourihane, M. Kowalski, N.G. Papadopoulos, J.-M. Wal, E.N.C. Mills, S. Vieths, IgE-mediated food allergy diagnosis: current status and new perspectives, Mol. Nutr. Food Res. 51 (2007) 135–147, https://doi.org/10.1002/mnfr.200600132.

[9] K. Sofinska, Z. Adamczyk, J. Barbasz, Mechanism of immunoglobulin G adsorption on polystyrene microspheres, Colloids Surf. B 137 (2016) 183–190, https://doi.org/10.1016/j.colsurfb.2015.07.037.

[10] F. Galisteo-González, J. Puig, A. Martín-Rodriguez, J. Serra-Domènech, R. Hidalgo-Alvarez, Influence of electrostatic forces on IgG adsorption onto polystyrene beads, Colloids Surf. B 2 (1994) 435–441, https://doi.org/10.1016/0927-7765(94)80008-1.

[11] S. Kochwa, M. Brownell, R.E. Rosenfield, L.R. Wasserman, Adsorption of proteins by polystyrene particles. I. Molecular unfolding and acquired immunogenicity of IgG, J. Immunol. 99 (1967) 981–986.

[12] J. Serra, J. Puig, A. Martin, F. Galisteo, M.J. Galvez, R. Hidalgo-Alvarez, On the adsorption of IgG onto polystyrene particles: electrophoretic mobility and critical coagulation concentration, Colloid Polym. Sci. 270 (1992) 574–583, https://doi.org/10.1007/BF00658288.

[13] P. Żeliszewska, M. Wasilewska, Z. Adamczyk, Monolayers of immunoglobulin G on polystyrene microparticles and their interactions with human serum albumin, J. Colloid Interface Sci. 490 (2017) 587–597, https://doi.org/10.1016/j.jcis.2016.11.090.

[14] C. Contado, L. Bregola, F. Dondi, Sedimentation field flow fractionation of immunoglobulin A coated polystyrene beads. Influence of carrier composition on complex characterization, J. Chromatogr. A 1169 (2007) 158–174, https://doi.org/10.1016/j.chroma.2007.08.069.

[15] L. Bregola, C. Contado, M. Martin, L. Pasti, F. Dondi, Precision in differential field-flow fractionation: a chemometric study, J. Sep. Sci. 30 (2007) 2760–2779, https://doi.org/10.1002/jssc.200700200.

[16] B. Langwost, K.D. Caldwell, Solid phase immune reactions as monitored by sedimentation field-flow fractionation, Chromatographia 34 (1992) 317–324, https://doi.org/10.1007/BF02268362.

[17] Y. Jiang, J.C. Giddings, R. Beckett, Direct measurement of protein adsorption on latex particles by sedimentation Field-flow fractionation, Proteins at Interfaces II, ACS Symposium Series, 602 (1995) 405–419, https://doi.org/10.1021/bk-1995-0602.ch029, Chapter 29.

[18] M.R. Nejadnik, W. Jiskoot, Measurement of the average mass of proteins adsorbed to a nanoparticle by using a suspended microchannel resonator, J. Pharm. Sci. 104 (2015) 698–704, https://doi.org/10.1002/jps.24206.

[19] N.C. Bell, C. Minelli, A.G. Shard, Quantitation of IgG protein adsorption to gold nanoparticles using particle size measurement, Anal. Methods 5 (2013) 4591–4601, https://doi.org/10.1039/c3ay40771c.

[20] N.A. Belsey, A.G. Shard, C. Minelli, Analysis of protein coatings on gold nanoparticles by XPS and liquid-based particle sizing techniques, Biointerphases 10 (2015)019012-1-019012-9https://doi.org/10.1116/1.4913566.

[21] R.J. Seidewand, J.R. Erickson, Multistage latex particle size analysis by disc centrifuge photosedimentometry, Polymer Eng. Sci 18 (1978) 1182–1185, https://doi.org/10.1002/pen.760181510.

[22] L. Shang, G.U. Nienhaus, In situ characterization of protein adsorption onto nanoparticles by fluorescence correlation spectroscopy, Acc. Chem. Res. 50 (2017) 387–395, https://doi.org/10.1021/acs.accounts.6b00579.

[23] R. Capomaccio, I.O. Jimenez, P. Colpo, D. Gilliland, G. Ceccone, F. Rossi, L. Calzolai, Determination of the structure and morphology of gold nanoparticle–HSA protein complexes, Nanoscale 7 (2015) 17653–17657, https://doi.org/10.1039/C5NR05147A.

[24] D. Vilela, M.C. González, A. Escarpa, Sensing colorimetric approaches based on gold and silver nanoparticles aggregation: chemical creativity behind the assay. A review, Anal. Chim. Acta 751 (2012) 24–43, https://doi.org/10.1016/j.aca.2012.08.043.

[25] D.V. Sotnikov, A.N. Berlina, V.S. Ivanov, A.V. Zherdev, B.B. Dzantiev, Adsorption of proteins on gold nanoparticles: one or more layers?, Colloids Surf. B 173 (2019) 557–563, https://doi.org/10.1016/j.colsurfb.2018.10.025.

[26] M. Shimpf, K.D. Caldwell, J.C. Giddings (Eds.), Field Flow Fractionation Handbook, Wiley-Interscience, New York, 2000.

[27] T. Allen, Particle Size Measurement, Ch.12 John Wiley & Sons, New York, 1975.

[28] K. Brugger, The particle size determination of pigments with the disc centrifuge, Powder Technol. 13 (1976) 215–221, https://doi.org/10.1016/0032-5910(76)85006-1.

[29] J.J. Kirkland, W.W. Yau, Simultaneous determination of particle size and density by sedimentation field flow fractionation, Anal. Chem. 55 (1983) 2165–2170, https://doi.org/10.1021/ac00263a037.

[30] M. Kamiti, D. Boldridge, L.M. Ndoping, E.E. Remsen, Simultaneous absolute determination of particle size and effective density of submicron colloids by disc centrifuge photosedimentometry, Anal. Chem. 84 (2012) 10526–10530, https://doi.org/10.1021/ac3022086.

[31] A. Neumann, W. Hoyer, M.W. Wolff, U. Reichl, A. Pfitzner, B. Roth, New method for density determination of nanoparticles using a CPS disc centrifugeTM, Colloids Surf. B 104 (2013) 27–31, https://doi.org/10.1016/j.colsurfb.2012.11.014.

[32] R. Beckett, J. Ho, Y. Jang, J.C. Giddings, Measurement of mass and thickness of adsorbed films on colloidal particles by sedimentation field-flow fractionation, Langmuir 7 (1991) 2040–2047, https://doi.org/10.1021/la00058a013.

[33] J.-T. Li, K.D. Caldwell, N. Rapoport, Surface properties of pluronic-coated polymeric colloids, Langmuir 10 (1994) 4475–4482, https://doi.org/10.1021/la00024a016.

[34] M. Andersson, K. Fromell, E. Gullberg, P. Artursson, K.D. Caldwell, Characterization of surface-modified nanoparticles for in vivo biointeraction. A sedimentation field flow fractionation study, Anal. Chem. 77 (2005) 5488–5493, https://doi.org/10.1021/ac050631h.

[35] ISO 13318-2: Determination of Particle Size Distribution by Centrifugal Liquid Sedimentation Methods—Part 2: Photocentrifuge Method, International Organization for Standardization, Geneva, Switzerland, 2007.

[36] ISO 13318-1: Determination of Particle Size Distribution by Centrifugal Liquid Sedimentation Methods—Part 1: General Principles and Guidelines, International Organization for Standardization, Geneva, Switzerland, 2001.

[37] N.C. Bell, C. Minelli, J. Tompkins, M.M. Stevens, A.G. Shard, Emerging techniques for submicrometer particle sizing applied to stöber silica, Langmuir 28 (2012) 10860–10872, https://doi.org/10.1021/la301351k.

[38] C. Minelli, R. Garcia-Diez, A.E. Sikora, C. Gollwitzer, M. Krumrey, A.G. Shard, Characterization of IgG-protein-coated polymeric nanoparticles using complementary particle sizing techniques, Surf. Interface Anal. 46 (2014) 663–667, https://doi.org/10.1002/sia.5381.

[39] S.M. North, E.R. Jones, G.N. Smith, O.O. Mykhaylyk, T. Annable, S.P. Armes, Adsorption of small cationic nanoparticles onto large anionic particles from aqueous solution: a model system for understanding pigment dispersion and the problem of effective particle density, Langmuir 33 (2017) 1275–1284, https://doi.org/10.1021/acs.langmuir.6b04541.

[40] J. Brandup, E.H. Immergut, E.A. Grulke, Polymer Handbook, forth ed., John Wiley & Sons, New York, 1999.

[41] J. Liu, P. Lester, S. Builder, S.J. Shire, Characterization of complex formation by humanized anti-IgE monoclonal antibody and monoclonal human IgE, Biochemistry 34 (33) (1995) 10474–10482, https://doi.org/10.1021/bi00033a020.

[42] J.K. Armstrong, R.B. Wenby, H.J. Meiselman, T.C. Fisher, The hydrodynamic radii of macromolecules and their effect on red blood cell aggregation, Biophys. J. 87 (6) (2004) 4259–4270, https://doi.org/10.1529/biophysj.104.047746.

[43] M.L. Quillin, B.W. Matthews, Accurate calculation of the density of proteins, Acta Cryst D56 (2000) 791–794, https://doi.org/10.1107/S090744490000679X.

[44] D. Mehn, F. Caputo, M. Rösslein, L. Calzolai, F. Saint-Antonin, T. Courant, P. Wick, D. Gilliland, Larger or more? Nanoparticle characteriza-

tion methods for recognition of dimers, RSC Adv. 7 (2017) 27747–27754, https://doi.org/10.1039/C7RA02432K.

[45] L.L. Bondoc Jr, S. Fitzpatrick, Size distribution analysis of recombinant adenovirus using disc centrifugation, J. Ind. Microbiol. Biotechnol. 20 (1998) 317–322, https://doi.org/10.1038/sj.jim.2900529.

[46] V. Volkov, V.A. Lapuk, R.L. Kayushina, E.V. Shtykova, E.Y. Varlamova, M. Malfois, D.I. Svergun, Low-resolution structure of immunoglobulins IgG1, IgM and rheumatoid factor IgM-RF from solution X-ray scattering data, J. Appl. Cryst. 36 (2003) 503–508, https://doi.org/10.1107/S0021889803005156.

[47] A.K. Trilling, J. Beekwilder, H. Zuilhof, Antibody orientation on biosensor surfaces: a minireview, Analyst 138 (2013) 1619–1627, https://doi.org/10.1039/C2AN36787D.

[48] N.G. Welch, J.A. Scoble, B.W. Muir, P.J. Pigram, Orientation and characterization of immobilized antibodies for improved immunoassays, Biointerphases 12 (2017) 02D301-1–02D301-13, https://doi.org/10.1116/1.4978435.

[49] L. Dávalos-Pantoja, J.L. Ortega-Vinuesa, D. Bastos-González, R. Hidalgo-Álvarez, Colloidal stability of IgG- and IgY-coated latex microspheres, Colloids Surf. B 20 (2001) 165–175, https://doi.org/10.1016/S0927-7765(00)00189-2.

[50] L.F. Tóth, Über die dichteste Kugellagerung, Math Zeitschrift 48 (1942) 676–684, https://doi.org/10.1007/BF01180035.

[51] Ž. Krpetić, A.M. Davidson, M. Volk, R. Lévy, M. Brust, D.L. Cooper, High-resolution sizing of monolayer-protected gold clusters by differential centrifugal sedimentation, ACS Nano 7 (2013) 8881–8890, https://doi.org/10.1021/nn403350v.

[52] J. Vörös, The density and refractive index of adsorbing protein layers, Biophys. J. 87 (1) (2004) 553–561, https://doi.org/10.1529/biophysj.103.030072.

[53] A.M. Davidson, M. Brust, D.L. Cooper, M. Volk, Sensitive analysis of protein adsorption to colloidal gold by differential centrifugal sedimentation, Anal. Chem. 89 (2017) 6807–6814, https://doi.org/10.1021/acs.analchem.7b01229.

[54] T. Nakamura, I. Sekigawa, H. Ogasawara, K. Mitsuishi, K. Hira, S. Ikeda, H. Ogawa, Expression of DNMT-1 in patients with atopic dermatitis, Arch. Dermatol. Res. 298 (2006) 253–256, https://doi.org/10.1007/s00403-006-0682-0.

[55] C. Gollwitzer, D. Bartczak, H. Goenaga-Infante, V. Kestens, M. Krumrey, C. Minelli, M. Pálmai, Y. Ramaye, G. Roebben, A. Sikora, Z. Varga, A comparison of techniques for size measurement of nanoparticles in cell culture medium, Anal. Methods 8 (2016) 5272–5282, https://doi.org/10.1039/c6ay00419a.